nature nanotechnology

Article

https://doi.org/10.1038/s41565-022-01256-4

Versatile full-colour nanopainting enabled by a pixelated plasmonic metasurface

Received: 27 January 2022

Accepted: 4 October 2022

Published online: 5 December 2022

Check for updates

Maowen Song[1,2,4], Lei Feng[1,2,4], Pengcheng Huo[1,2], Mingze Liu[1,2], Chunyu Huang[1], Feng Yan[1,3], Yan-qing Lu[1,2] ✉ & Ting Xu[1,2] ✉

The growing interest to develop modern digital displays and colour printing has driven the advancement of colouration technologies with remarkable speed. In particular, metasurface-based structural colouration shows a remarkable high colour saturation, wide gamut palette, chiaroscuro presentation and polarization tunability. However, previous approaches cannot simultaneously achieve all these features. Here, we design and experimentally demonstrate a surface-relief plasmonic metasurface consisting of shallow nanoapertures that enable the independent manipulation of colour hue, saturation and brightness by individually varying the geometric dimensions and orientation of the nanoapertures. We fabricate microscale artworks using a reusable template-stripping technique that features photorealistic and stereoscopic impressions. In addition, through the meticulous arrangement of differently oriented nanoapertures, kaleidoscopic information states can be decrypted by particular combinations of incident and reflected polarized light.

Dyes and pigments are the most commonly used materials to render colours in our daily life as they can absorb certain wavelengths from the visible spectrum and reflect the remaining parts[1]. However, they are not chemically stable, especially at high temperatures or when exposed to intense ultraviolet light, and the colour gamut is very limited. Owing to the fact that some structures that occur artificially are fine enough to interfere with light and produce a vibrant appearance of historic artworks, structural colouration becomes an alternative approach to tackle the obstacles of dyes and pigments[2]. With the advancement of nanofabrication technology, plasmonic nanostructures were recently precisely engineered and crafted to tailor the spectrum at an unprecedented level[3–13]. Thus far, highly dense arrangements of nanodisks[14–17], metal–insulator–metal nanopatch arrays[18–22] and periodically aligned nanowires[23–27] suggest exciting routes towards producing colours. However, the colour gamut is limited and the spectral linewidth is still relatively broad as metallic loss and surface roughness play important roles in the visible regime[1].

Employing high-index dielectric nanostructures seems to be an alternative strategy to circumvent these challenges[28–35]. Through the well-designed electric and magnetic Mie resonances[36–39], the spectra purity and colour performance of dielectric competitors are generally presented as superior to those of plasmonic colour filtering devices. When integrated with a low-index impedance matching layer, the spectral linewidth can be narrowed even further. However, this approach fails to control the colour brightness, which leads to the absence of chiaroscuro in an image. Recently, a metasurface with silicon rectangular nanofins patterned on a fused SiO_2 substrate was demonstrated to simultaneously tune hue, saturation and brightness[40]. Nevertheless, such a spatial multiplexing strategy severely deteriorates the filtered spectrum bandwidth, and the high aspect ratio (~1:15) surface features pose great challenges for its nanofabrication.

In this work, we show a surface-relief plasmonic metasurface that combines a number of features simultaneously, which include a high colour saturation, wide gamut palette, chiaroscuro presentation and polarization tunability. The ultrashallow nanoapertures embedded

[1]National Laboratory of Solid-State Microstructures and Collaborative Innovation Center of Advanced Microstructures, Nanjing University, Nanjing, China. [2]Jiangsu Key Laboratory of Artificial Functional Materials, Key Laboratory of Intelligent Optical Sensing and Manipulation, College of Engineering and Applied Sciences, Nanjing University, Nanjing, China. [3]School of Electronic Science and Engineering, Nanjing University, Nanjing, China. [4]These authors contributed equally: Maowen Song, Lei Feng. ✉e-mail: yqlu@nju.edu.cn; xuting@nju.edu.cn

https://doi.org/10.1038/s41565-022-01256-4

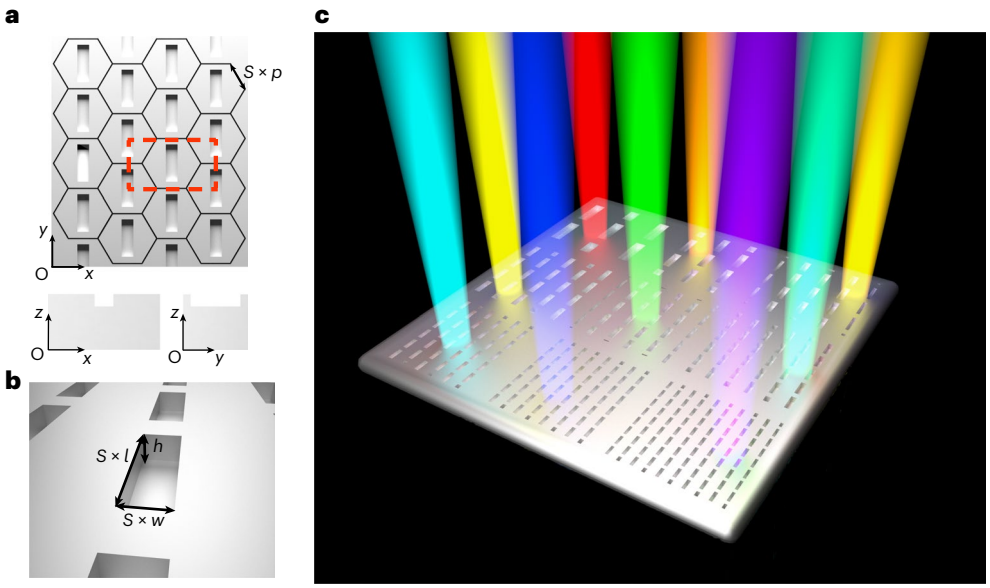

Fig. 1 | Schematic of the surface-relief silver metasurface. a, Top view of the 4 × 4 metasurface unit cells of lattice side length *p*. The rectangular region enclosed by the red dashed line is the unit cell used in our simulation. Resonance frequencies were tuned by multiplying the unit cell lateral dimensions by a scaling factor *S*. Insets: the *xz* and *yz* cross-section views of the unit cell nanoaperture. **b**, Perspective view of a single unit cell that contains a nanoaperture with a size of length (*l*), width (*w*) and thickness (*h*) embedded in optically thick silver film. **c**, Schematic diagram of the pixelated metasurface, which consists of a two-dimensional array of nanoapertures with resonant wavelengths tuned over the visible region.

in the optically thick silver film that composes metasurface pixels are manufactured by a reusable template-stripping technique, and hence potentially enable low-cost mass production. As proof-of-concept demonstrations, we fabricated several metasurface artworks with photorealistic impressions and subtle renderings of the texture details of the original oil paintings. Besides nanopainting functionality, polarization of light provides the possibility to tune a picture. Through the meticulous arrangement of differently oriented nanoapertures, kaleidoscopic images can be selectively decrypted without any 'cross-talk' effect.

Design of pixelated plasmonic metasurface

Individual metapixels of the proposed metasurface contain an array of anisotropic nanoapertures embedded in optically thick silver film, as shown in Fig. 1a. The lattice side length *p* of hexagonally arranged nanoapertures to form metasurface pixels is 160 nm. For each nanoaperture (Fig. 1b), length (*l*), width (*w*) and thickness (*h*) are optimized as $l = 200$ nm, $w = 60$ nm and $h = 40$ nm; the following transverse scaling and experimental design are all based on these parameters. This configuration is capable of converting the diagonally oriented (45° with respect to the long axis of the nanoaperture) linearly polarized (LP) visible light into other polarization states. Importantly, a complete 90° optical rotation effect can be readily achieved with a high reflection efficiency when the geometric dimensions of the nanoapertures are judiciously optimized. As a result, the designed metasurface exhibits a single sharp reflectance peak in the optical spectrum and highly suppresses the reflectance at other off-resonance wavelengths under cross-linear-polarization conversion, which remarkably increases the colour saturation and gamut. In addition, such an architecture allows for a straightforward resonance tuning via multiplying the unit-cell lateral dimensions by a scaling factor *S*, and the linear tunability of the spectral peak positions can cover the entire visible region. The concept of a colour filtering effect by a two-dimensional array of metasurface pixels is schematically illustrated in Fig. 1c. The quantitative comparison of colour performances between our work and other recent papers is listed in Supplementary Section 1.

High colour saturation and wide colour gamut

Plasmonic colours usually suffer from low saturation and limited gamut due to the ohmic loss of metals[37]. In addition, when surface plasmons travel along a rough metal surface, they can easily become radiative due to scattering, which further weakens the plasmonic resonance effect. In this work, silver was chosen as the constituent material of the metasurface due to its excellent optical properties, which support strong plasmon resonances with a relatively low loss[41]. Besides, to obtain an ultrasmooth surface of the silver nanostructures, the nanopatterns were fabricated on the silicon via electron-beam lithography and then transferred to silver film by a reusable template-stripping technique, as shown in Supplementary Fig. 1. The detailed fabrication approach is described in Methods.

To evaluate the colour performance of this metasurface, we first numerically investigated the reflectance spectra under cross-linear-polarization conversion by means of a frequency domain finite element method. The unit-cell built-in simulation is shown in Fig. 1b with a red dashed line. The frequency-dependent permittivity of silver was obtained from the data measured by Johnson and Christy[42]. The modelled metasurface was illuminated by a normally incident LP light with a polarization angle of 45° with respect to the *x* direction. The left panel in Fig. 2a presents the calculated reflectance spectra under cross-polarization conversion with the scaling factor *S* varying from 1.20 to 2.65. It can be observed that each individual spectrum exhibits a sharp peak at particular wavelengths without an additional resonance background. As the lateral size increases, the position of the reflectance peak redshifts from 452 to 682 nm (Supplementary Fig. 2). The dependences of the simulated cross-polarization reflection spectra for the proposed nanoaperture array with different structural parameters were also investigated (Supplementary Fig. 3). Remarkably, by introducing more groups of nanoapertures with various lengths and widths, the narrowest full width at half maximum of the reflection spectra reached sub-10 nm (Supplementary Fig. 4). The right panel in Fig. 2a shows the experimentally measured spectra, which closely resemble those of the simulated results. Some slight differences result from the shape distortion at the fabricated nanoaperture corners, as well as changes

https://doi.org/10.1038/s41565-022-01256-4

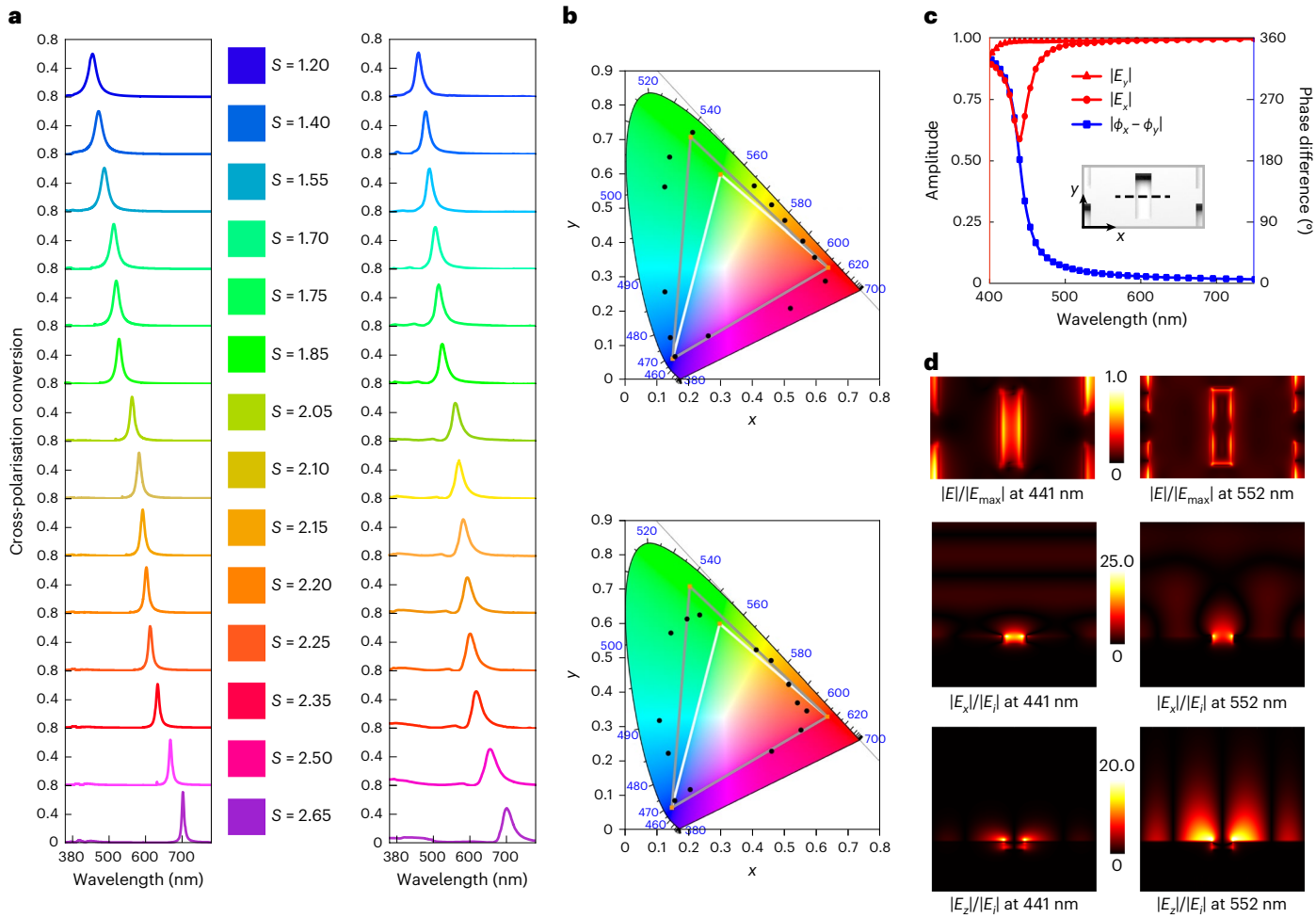

Fig. 2 | Experimental colour hues of the metasurface and theoretical fundamentals. a, Simulated (left) and experimentally (right) measured reflectively cross-polarized spectra of the metasurface and the corresponding colours when the scaling factor varies from 1.20 to 2.65. **b**, Chromatic coordinates in the CIE 1931 diagram obtained from the simulated (top) and measured (bottom) spectra. The regions enclosed by grey and white lines present Adobe RGB space and sRGB space, respectively. **c**, Simulated reflective amplitude spectra (red curve) and phase difference (blue curve) between the *x* and *y* components. Inset: the structural unit cell utilized in the electric field distribution analysis. **d**, Simulated electric field distributions of the structural unit cell with $S = 1$ (left panels) and 2 (right panels) at corresponding resonant wavelengths (441 and 552 nm). Top row: total electric field intensity distribution at the surface of the nanoapertures array. All the values are normalized to their respective maxima. Middle row: *x*-component electric field intensity distribution on the *xz* plane. Bottom row: *z*-component electric field intensity distribution on the *xz* plane.

in the optical properties of nanostructured silver. We calculated the colours via colour-matching functions defined by the CIE (International Commission on Illumination) and the corresponding results are presented in the column between the simulated and measured spectra of Fig. 2a. To have a better understanding of the ultrahighly saturated colours and wide gamut, the corresponding chromatic coordinates are plotted in a CIE 1931 chromaticity diagram, as shown in Fig. 2b. From the simulation results, the colour gamut could achieve about a 182% standard red, green and blue (sRGB) space and a 134% Adobe RGB space (details in Supplementary Section 6). The chromatic coordinates that correspond to the experimentally measured spectra display a reasonable agreement with their simulation counterparts. In the experiment, the colour gamut approximately achieved a 148% sRGB space and a 109% Adobe RGB space. The smaller gamut can be understood by the fact that the wider spectral linewidth and unexpected reflectance at short wavelengths decreases the colour saturation.

To investigate the physical mechanism behind the generation of ultrasharp reflection spectra under cross-polarization conversion, the absorption spectra of *x*-polarized and *y*-polarized light were theoretically investigated (Supplementary Section 7). A strong spectral change of *x*-polarized light was observed at the wavelength of plasmonic resonance with the spectrum of *y*-polarized light relatively flat. As a result, the reflective amplitude of the *x*-component electric field spectrum underwent a sharp dip at a wavelength of 441 nm when a 45° polarized LP light normally illuminated the metasurface with an *S* of 1, as shown in Fig. 2c. It can be concluded that the plasmonic resonance caused this birefringence effect of our surface-relief silver metasurface and the 180° phase difference between the orthogonal linear polarizations depicted by the blue curve indicates the realization of a complete 90° optical rotation[43]. A detailed deduction as to the relationship between the reflected intensity and polarizer–analyser angle combinations are given in Supplementary Section 8. Figure 2d presents the electric field distributions in a structural unit cell with $S = 1$ and 2 at their corresponding resonant wavelengths (441 nm and 552 nm, respectively). The electric field is obviously enhanced at the silver–air interface inside the void and coupled to the neighbouring nanoapertures, which verifies the existence of both delocalized and localized plasmon modes[44]. To have a clear visualization about the contributions of each mode, the electric field profiles at the vertical cross-section (along the black dashed line in the structural unit cell in Fig. 2c) with $S = 1$ and 2 are plotted. When

https://doi.org/10.1038/s41565-022-01256-4

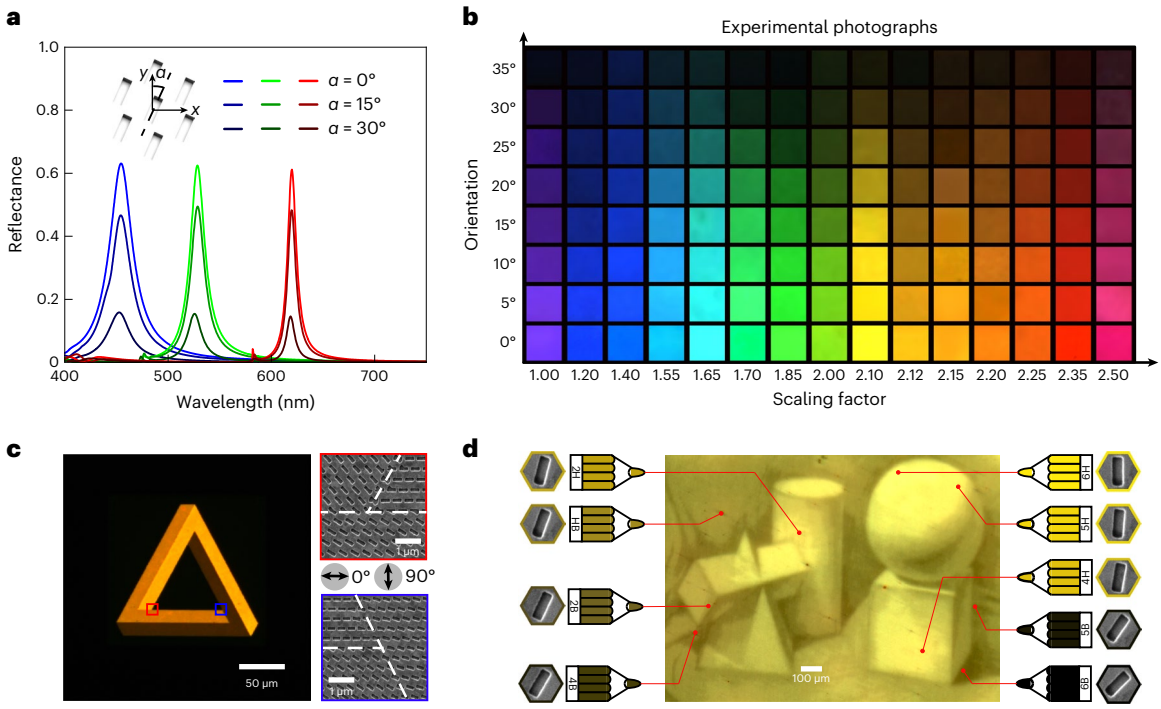

Fig. 3 | Plasmonic sketch with continuous colour brightness tuning. **a**, Simulated reflectance spectra of the blue, green and red pixels with the orientation of the nanoapertures varying from 0 to 30°. **b**, Colour palette photographed by a CCD camera with varying scaling factors and orientations of nanoaperture. Each sample is 100 μm × 100 μm. **c**, Experimental optical micrograph of the Penrose triangle on orthogonally polarized incident and reflected light. Insets: SEM images of the fabricated Penrose-patterned metasurface taken in the demarcation regions between differently oriented nanoapertures. The circles between the two SEM images represent the polarizer and analyser angles with corresponding numerals. **d**, Experimental optical image of a sketch. Differently oriented nanoapertures behave as pencils marked with various B or H values. The larger the Arabic numerals in front of the B (H), the lower (higher) the brightness.

the centre distance between neighbouring nanoapertures was 277 nm ($S = 1$), most x- and z-component electric fields were strongly localized at the corners and edges of the nanoaperture, which indicates that the localized plasmon mode dominated the optical rotation effect. The delocalized plasmon mode cannot exist when the lattice constant of the metallic nanostructure array is at a subwavelength scale. However, this effect becomes apparent as the lateral size of the metasurface increases. As presented in the bottom-right of Fig. 4d, the z-component electric field became more intense and the coupling between neighbouring nanoapertures was enhanced, which is a quintessential feature of a delocalized plasmon mode. Accordingly, the colour performance was a bit dependent on the viewing angles (Supplementary Section 9) and the minimal pixel size was limited to a few micrometres as a periodic arrangement in each individual pixel was necessary to ensure the coupling effect required to produce high saturation colours.

Chiaroscuro presentation and plasmonic sketch

The proposed surface-relief plasmonic metasurface can also allow the independent control of colour brightness. When a LP light illuminates the nanoapertures with a rotation angle of α (with respect to the y direction here), the reflectance of cross-polarizations is proportional to $\cos^2\alpha$ based on the Malus law. Therefore, the colour brightness can be readily altered by rotating the orientation of the nanoaperture. Figure 3a shows the reflectance of the cross-polarization spectra of blue, green and red colour pixels with different orientations that varied from 0 to 30°. Interestingly, the spectral profiles of the RGB pixels remained identical but with a decreasing magnitude, which demonstrates a continuous modification of the colour brightness without changes of hue and saturation. Such a feature benefits from the hexagonal lattice arrangement, which exhibits a higher azimuthal symmetry in the design of periodic nanostructures (Supplementary Section 10). Figure 3b presents photographs of the optical images of 120 samples with different scaling factors and oriented nanoapertures. It can be observed that the colour hue gradually varied from purple to magenta with increases of S from 1 to 2.5. In addition, an ultrasmooth colour brightness transition can be realized when the orientation of the nanoaperture rotates from 0 to 35° with a step of 5°. All the results were obtained by photographing the metasurface with a chromatic CCD (charge-coupled device) camera integrated with an optical microscope. The detailed optical set-up is schematically shown in Supplementary Fig. 8.

By tuning the colour brightness with a fixed hue, a shadow rending effect emerges and endows the painting with stronger space and stereo perceptions. As a proof-of-concept demonstration, a 'Penrose triangle' was selected as a target image for painting. Figure 3c shows the experimentally photographed result and enlarged scanning electron microscopy (SEM) images of the demarcation between differently oriented nanoapertures. When incident and reflected polarizations were at 0 and 90° with respect to the x direction, the triangle painted with light appears to be a solid object consisting of three straight bars that meet pairwise at 90° angles at the vertices of the triangle. Such a vivid multidimensional visual effect is caused by the distinct bright and dark contrast in the captured picture. The SEM images showcase visually uniform dense patterns, which guarantee that the orange-coloured Penrose triangle sharply contrasts the black background even at the corners and edges.

As the plasmonic metasurface is able to smoothly control the colour brightness, it can also be used to draw microscale sketches. Conventional pencils used to draw sketches are marked with B (black) or H (hard). The larger the Arabic numerals in front of the B, the softer the graphite, which is utilized to draw shady parts and corresponds

https://doi.org/10.1038/s41565-022-01256-4

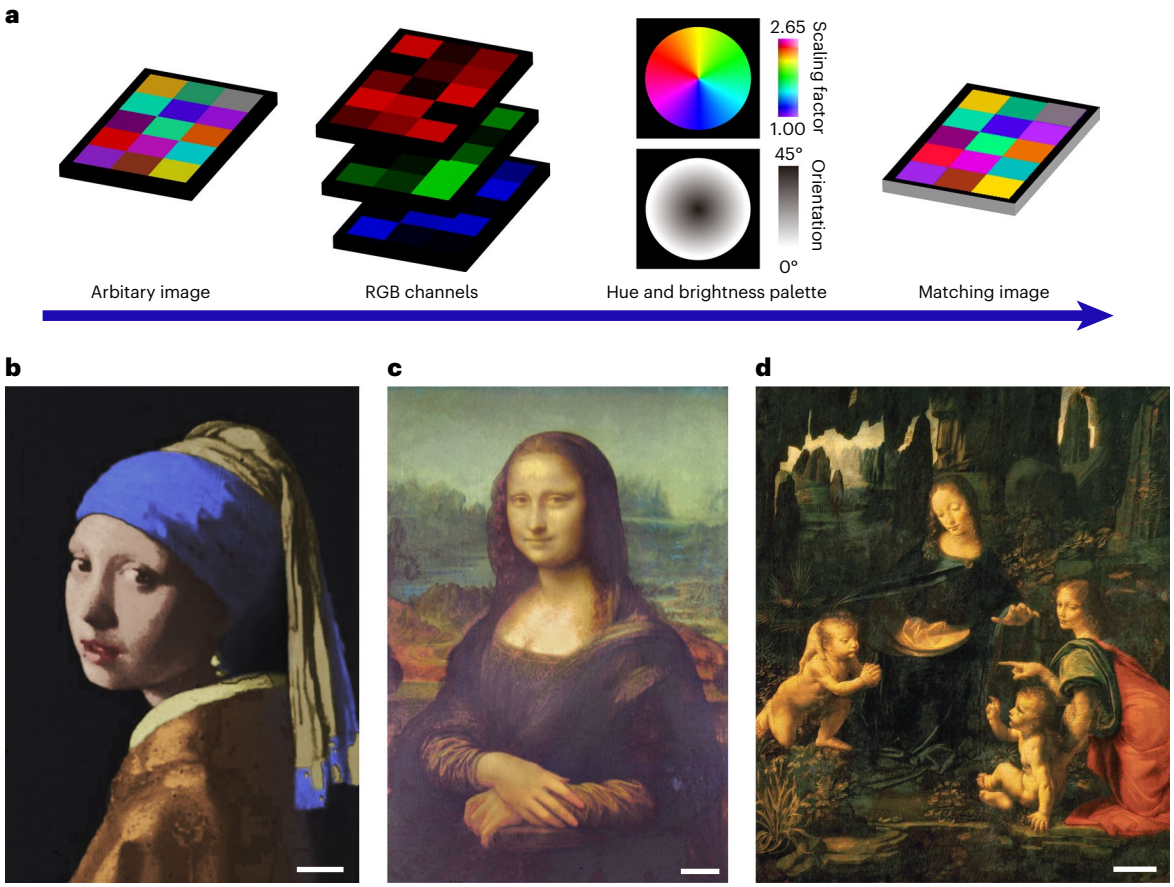

Fig. 4 | Photorealistic plasmonic full-colour nanopainting. a, Schematic diagram of designing a patterned metasurface for simultaneously realizing various colour hues and brightness. **b**–**d**, Experimentally captured optical photographs of the metasurface-based artworks *Girl with a Pearl Earring* (**b**), *Mona Lisa* (**c**) and *Virgin of the Rocks* (**d**). The images show ultrasmooth transitions between the different colour hues and brightness by using our plasmonic colouring approach. Scale bars, 200 μm.

to oriented nanoapertures with low-brightness colours; the larger the Arabic numerals in front of the H, the harder the texture, which is fit for plotting areas with a brighter lustre and corresponds to oriented nanoapertures with high-brightness colours. In our case, nanoapertures with a given orientation can be analogous to a microscale pencil, which renders a unique colour luminance when photographed with orthogonal polarizer–analyser combinations. Figure 3d presents an optical image of a specially designed and fabricated metasurface that portrays several geometric objects. As observed, our plasmonic sketching technique enables the production of realistic images with ultrasmooth greyscale transitions on the surface of objects, and nicely furnishes detailed levels in the tone of the colour brightness and presents a stereoscopic impression.

All-in-one solution for high-performance colour painting

By encoding the colour hue and brightness information into the geometric-dimension- and orientation-varied nanoapertures, the printed image enables a highly saturated full-colour presentation and stereoscopic image impression on white illumination. Based on this characteristic, we designed a parameter-matching approach to reproduce microscale full-colour paintings, as shown in Fig. 4a. First, a target image was first split into RGB channels. Colour values from each individual pixel of the arbitrary image were matched to the closest available additive colours by finding the minimal difference between the RGB values obtained from the target image and the colour palette of our metasurface. Subsequently, a self-written script was used to determine the scaling factor and orientation of the nanoaperture in each pixel according to a one-to-one relationship between the spectral and spatial information.

As a demonstration of our plasmonic nanopainting technique, we selected three famous artworks as target images. Figure 4b–d showcases the experimental photographs of three famous artworks *Girl with a Pearl Earring*, *Mona Lisa* and *Virgin of the Rocks*. The reproduced *Girl with a Pearl Earring* (Fig. 4b) presents that the girl wears a blue turban, yellowish draperies and a gold jacket with vibrant colours and seamless brightness transitions. The *Mona Lisa*, Leonardo's most famous artwork, is renowned for its mastery of technical innovations in the presentation of the mysterious smile. It was found that Leonardo utilized multilayers of pigment on Mona Lisa's face, especially in the darker area, to realize a sfumato and chiaroscuro effect[45]. For our metasurface, such complicated steps can be substituted by judiciously optimized silver nanoapertures with different lateral sizes and orientations. As a result, the enigmatic gaze, mysterious smile and stereoscopic sense of mountains, rivers and trees in the background are nicely presented (Fig. 4c). Finally, the famous artwork *Virgin of the Rocks* exhibits many complicated details and is regarded as a perfect example of Leonardo's sfumato technique. Figure 4d presents the experimentally photographed image of *Virgin of the Rocks*. Continuously rotated nanoapertures model the elusive and photorealistic rendering of the human face. Rich details, such as the textures of craggy rocks, strips in the red robe and tiny flowers on the footstep, are nicely reproduced through contrasts of light and shadow. Comparison between the target oil paintings and experimentally optical photographs are presented in

https://doi.org/10.1038/s41565-022-01256-4

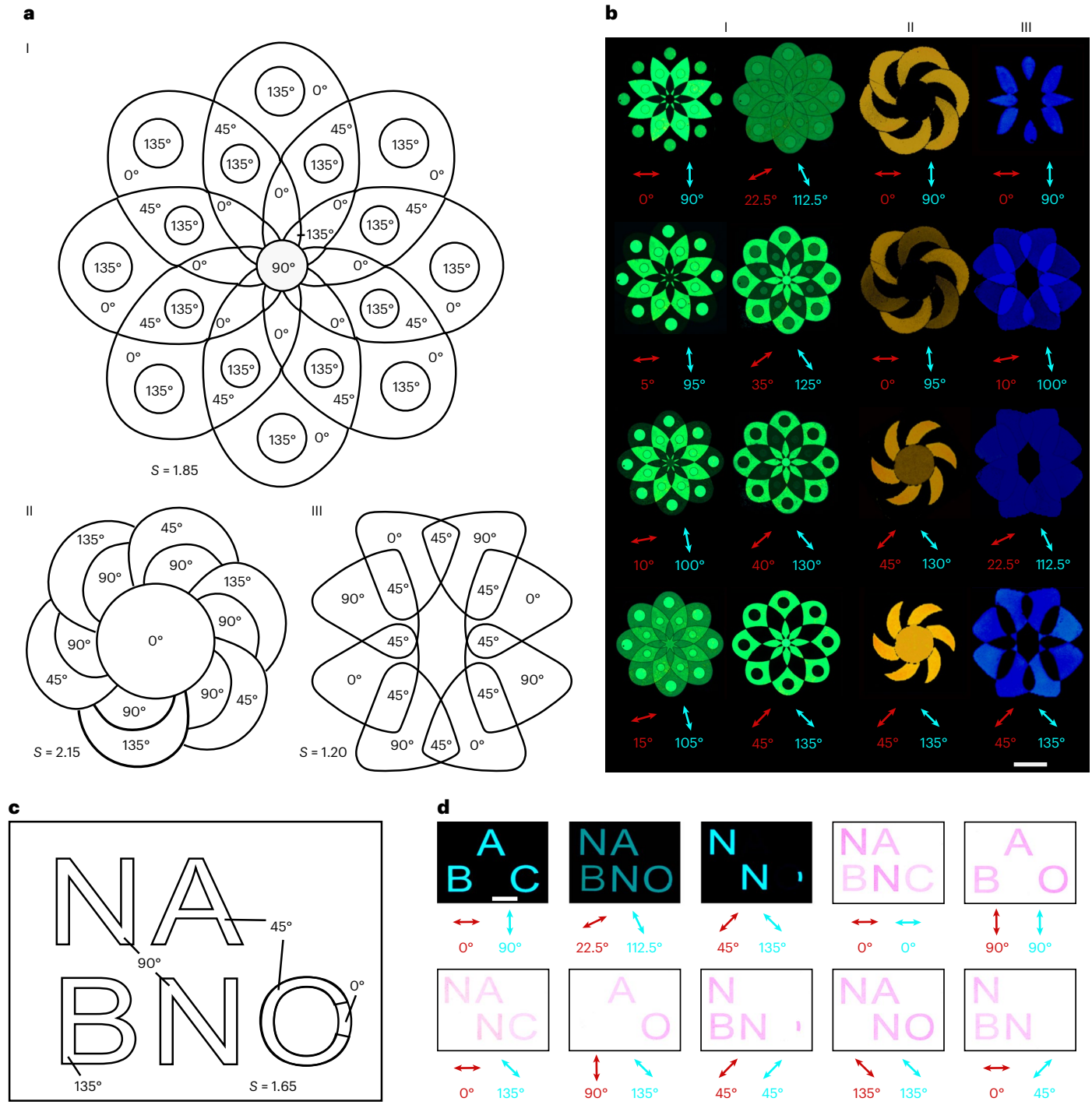

Fig. 5 | Experimental proof-of-concept for the steganography technique. **a**, Schematic of the steganographic flower pattern presented with different numerals that indicate the corresponding nanoaperture orientations. The scaling factors of the nanoapertures in patterns (i), (ii) and (iii) are 1.85, 2.15 and 1.20, respectively. **b**, Experimental optical micrographs on rotating polarizer and analyser. The highlighted arrows and corresponding numerals below each individual photograph represent the angles of the polarizer (red) and analyser (blue). Scale bar, 50 μm. **c**, Schematic of the steganographic information pattern presented with different numerals that indicate different nanoaperture orientations. **d**, Experimentally captured optical micrographs of the steganographic information display. Different information states can be clearly decrypted under special combinations of polarizer and analyser angles. Given the uniformity of the background, the exposure time under polarization combinations of (0°, 135°), (90°, 135°) and (0°, 45°) are slightly extended. Scale bar, 40 μm.

Supplementary Fig. 9. Additionally, to demonstrate the reusability of the silicon painting mould, we fabricated several *Mona Lisa* patterned metasurfaces from the same mould, as presented in Supplementary Fig. 10.

Polarization-tunable kaleidoscopic steganography

Owing to the fact that the proposed metasurface consists of periodic arrangements of rectangular-shaped silver nanoapertures attached

to an optically thick silver film, the appearance of colour performance can be readily tuned by altering the incident or reflected polarization states. Such a characteristic opens up an avenue for advanced steganography—a technique that can conceal an image within another image. To demonstrate the plasmonic steganography technique with kaleidoscopic colour image switching, a variety of flower-like patterns were designed, as depicted in Fig. 5a. Figure 5b presents the experimentally photographed images under different polarizer–analyser combinations. Taking pattern (i) as an example: a clear-cut green flower with eight peripheral speckles sharply contrasts with a black background when the polarizer and analyser were set at 0 and 90°, respectively. When both the polarizer and analyser were rotated in the anticlockwise direction synchronously, the green flower underwent a dynamic pattern change with the disappearance of the peripheral speckles and the emergence of petals. Such an animation-like alternation resulted from the special design that colours produced from the areas occupied by 0°- and 90°-oriented nanoapertures gradually matched those from the 45°- and 135°-oriented nanoapertures. A flower with a uniform green colour was generated when the polarizer and analyser were rotated to 22.5 and 112.5°. Further rotating both the polarizer and analyser in the anticlockwise direction engendered the appearance of a totally different flower. Based on a similar principle, more distinct images were revealed under other states of polarizer–analyser combinations (see the results from patterns (ii) and (iii) in Fig. 5a), which largely increased the information capacity of our metasurface as a novel kind of steganography technique. To further demonstrate the capability of encoding various information states into the same pattern, the logo 'NABNO' pattern was designed and formed by nanoapertures with those four different orientations, as depicted in Fig. 5c. Figure 5d showcases the dynamic optical performance of our patterned metasurface. All the letters that constituted the pattern exhibited no discernible discrepancy under optical microscopy. The special information state could only be observed from the diverse text phrases when the unique polarizer–analyser combination was provided. Evidently, the experimentally photographed images showed no mixture of the undesired colour displays intended for other polarizer–analyser combinations, which is ideally suited for highly secure information encryption. The underlying physics, design principle and information-revealing manner are explained in details in Supplementary Section 14.

Conclusion

In this work, we propose a silver nanoaperture metasurface that offers the prospects of versatile full-colour nanopainting techniques with outstanding colour performances. The nanoaperture metasurface supports the excitation of both delocalized and localized plasmon modes. The delocalized one can produce ultrasharp reflection spectrum peaks, which leads to the generation of high-saturation colours. We united differently oriented nanoapertures to modulate the colour properties and mimicked conventional sketching and oil-painting techniques to obtain experimentally photographed microscale images that vividly showcase photorealistic and stereoscopic impressions. Besides, ten distinct information states can be encoded and revealed from the patterned metasurface only when the unique polarizer–analyser combination is provided, which thus exhibits great potentials in steganography and anticounterfeiting techniques.

One thing should be noted here is that the delocalized plasmon mode is sensitive to the incident angle, which means the metasurface has limited viewing angles, especially for longer wavelengths. Therefore, how to design the nanostructures with a large viewing angle while still maintaining the other colour performances remains a challenge. One approach is the accurate determination of the most suitable topology and geometric parameters for nanostructures from a hyperdimensional parameter space. Fortunately, the recently developed machine-learning-assisted photonic structure design approaches are promising to solve such a multiobjective optimization problem[46–48]. By merging topology optimization with generative adversarial networks, a faster global parameter search and optimization over hyperdimensional parametric landscapes can be realized. Additionally, a gradient descent algorithm can also be employed to optimize the structural parameters of the metasurface to achieve a better colour performance[49]. Therefore, through combining these promising design approaches to broaden the scope of optimal design, we envision our pixelated colour metasurface platform will be fit for a wide range of photonic and optoelectronic applications.

Online content

Any methods, additional references, Nature Portfolio reporting summaries, source data, extended data, supplementary information, acknowledgements, peer review information; details of author contributions and competing interests; and statements of data and code availability are available at https://doi.org/10.1038/s41565-022-01256-4.

References

1. Kristensen, A. et al. Plasmonic colour generation. *Nat. Rev. Mater.* **2**, 16088 (2016).
2. Song, M. et al. Colors with plasmonic nanostructures: a full-spectrum review. *Appl. Phys. Rev.* **6**, 041308 (2019).
3. Barnes, W. L., Dereux, A. & Ebbesen, T. W. Surface plasmon subwavelength optics. *Nature* **424**, 824–830 (2003).
4. Luo, X., Tsai, D., Gu, M. & Hong, M. Extraordinary optical fields in nanostructures: from sub-diffraction-limited optics to sensing and energy conversion. *Chem. Soc. Rev.* **48**, 2458–2494 (2019).
5. Li, Y., van de Groep, J., Talin, A. A. & Brongersma, M. L. Dynamic tuning of gap plasmon resonances using a solid-state electrochromic device. *Nano Lett.* **19**, 7988–7995 (2019).
6. Chowdhury, S. N. et al. Lithography-free plasmonic color printing with femtosecond laser on semicontinuous silver films. *ACS Photon.* **8**, 521–530 (2020).
7. Huang, Y.-W. et al. Aluminum plasmonic multicolor meta-hologram. *Nano Lett.* **15**, 3122–3127 (2015).
8. Ellenbogen, T., Seo, K. & Crozier, K. B. Chromatic plasmonic polarizers for active visible color filtering and polarimetry. *Nano Lett.* **12**, 1026–1031 (2012).
9. Neubrech, F., Duan, X. & Liu, N. Dynamic plasmonic color generation enabled by functional materials. *Sci. Adv.* **6**, eabc2709 (2020).
10. Duan, X., Kamin, S. & Liu, N. Dynamic plasmonic colour display. *Nat. Commun.* **8**, 14606 (2017).
11. Zhu, X., Vannahme, C., Højlund-Nielsen, E., Mortensen, N. A. & Kristensen, A. Plasmonic colour laser printing. *Nat. Nanotechnol.* **11**, 325–329 (2016).
12. Xue, J. et al. Perturbative countersurveillance metaoptics with compound nanosieves. *Light Sci. Appl.* **8**, 101 (2019).
13. Yang, Z., Ji, C., Cui, Q. & Guo, L. J. High-purity hybrid structural colors by enhancing optical absorption of organic dyes in resonant cavity. *Adv. Opt. Mater.* **8**, 2000317 (2020).
14. Clausen, J. S. et al. Plasmonic metasurfaces for coloration of plastic consumer products. *Nano Lett.* **14**, 4499–4504 (2014).
15. Esposito, M. et al. Symmetry breaking in oligomer surface plasmon lattice resonances. *Nano Lett.* **19**, 1922–1930 (2019).
16. Joo, W.-J. et al. Metasurface-driven OLED displays beyond 10,000 pixels per inch. *Science* **370**, 459–463 (2020).
17. Kumar, K. et al. Printing colour at the optical diffraction limit. *Nat. Nanotechnol.* **7**, 557–561 (2012).
18. Xu, T., Wu, Y.-K., Luo, X. & Guo, L. J. Plasmonic nanoresonators for high-resolution colour filtering and spectral imaging. *Nat. Commun.* **1**, 59 (2010).
19. Wang, H. et al. Full color generation using silver tandem nanodisks. *ACS Nano* **11**, 4419–4427 (2017).

20. Rezaei, S. D. et al. Wide-gamut plasmonic color palettes with constant subwavelength resolution. *ACS Nano* **13**, 3580–3588 (2019).
21. Roberts, A. S., Pors, A., Albrektsen, O. & Bozhevolnyi, S. I. Subwavelength plasmonic color printing protected for ambient use. *Nano Lett.* **14**, 783–787 (2014).
22. Goh, X. M. et al. Three-dimensional plasmonic stereoscopic prints in full colour. *Nat. Commun.* **5**, 5361 (2014).
23. Tan, S. J. et al. Plasmonic color palettes for photorealistic printing with aluminum nanostructures. *Nano Lett.* **14**, 4023–4029 (2014).
24. Shaltout, A. M., Kim, J., Boltasseva, A., Shalaev, V. M. & Kildishev, A. V. Ultrathin and multicolour optical cavities with embedded metasurfaces. *Nat. Commun.* **9**, 2673 (2018).
25. Hail, C. U., Schnoering, G., Damak, M., Poulikakos, D. & Eghlidi, H. A plasmonic painter's method of color mixing for a continuous red–green–blue palette. *ACS Nano* **14**, 1783–1791 (2020).
26. Lee, J. S. et al. Ultrahigh resolution and color gamut with scattering-reducing transmissive pixels. *Nat. Commun.* **10**, 4782 (2019).
27. Wu, Y.-K., Hollowell, A. E., Zhang, C. & Guo, L. J. Angle-insensitive structural colours based on metallic nanocavities and coloured pixels beyond the diffraction limit. *Sci. Rep.* **3**, 1194 (2013).
28. Proust, J., Bedu, F., Gallas, B., Ozerov, I. & Bonod, N. All-dielectric colored metasurfaces with silicon Mie resonators. *ACS Nano* **10**, 7761–7767 (2016).
29. Li, Q., Wu, T., van de Groep, J., Lalanne, P. & Brongersma, M. L. Structural color from a coupled nanowire pair beyond the bonding and antibonding model. *Optica* **8**, 464–470 (2021).
30. Dong, Z. et al. Printing beyond sRGB color gamut by mimicking silicon nanostructures in free-space. *Nano Lett.* **17**, 7620–7628 (2017).
31. Sun, S. et al. All-dielectric full-color printing with TiO_2 metasurfaces. *ACS Nano* **11**, 4445–4452 (2017).
32. Tittl, A. et al. Imaging-based molecular barcoding with pixelated dielectric metasurfaces. *Science* **360**, 1105 (2018).
33. Huo, P. et al. Photorealistic full-color nanopainting enabled by a low-loss metasurface. *Optica* **7**, 1171 (2020).
34. Koshelev, K. & Kivshar, Y. Dielectric resonant metaphotonics. *ACS Photon.* **8**, 102–112 (2021).
35. Bao, Y. et al. Coherent pixel design of metasurfaces for multidimensional optical control of multiple printing-image switching and encoding. *Adv. Funct. Mater.* **28**, 1805306 (2018).
36. Zhou, J. et al. Visualizing Mie resonances in low-index dielectric nanoparticles. *Phys. Rev. Lett.* **120**, 253902 (2018).
37. Yang, W. et al. All-dielectric metasurface for high-performance structural color. *Nat. Commun.* **11**, 1864 (2020).
38. Yang, B. et al. Ultrahighly saturated structural colors enhanced by multipolar-modulated metasurfaces. *Nano Lett.* **19**, 4221–4228 (2019).
39. Yang, J. H. et al. Structural colors enabled by lattice resonance on silicon nitride metasurfaces. *ACS Nano* **14**, 5678–5685 (2020).
40. Bao, Y. et al. Full-colour nanoprint-hologram synchronous metasurface with arbitrary hue–saturation–brightness control. *Light Sci. Appl.* **8**, 95 (2019).
41. Jiang, M. et al. Patterned resist on flat silver achieving saturated plasmonic colors with sub-20-nm spectral linewidth. *Mater. Today* **35**, 99–105 (2020).
42. Johnson, P. B. & Christy, R. W. Optical constants of the noble metals. *Phys. Rev. B* **6**, 4370–4379 (1972).
43. Wu, S. et al. Enhanced rotation of the polarization of a light beam transmitted through a silver film with an array of perforated s-shaped holes. *Phys. Rev. Lett.* **110**, 207401 (2013).
44. Kelf, T. A. et al. Localized and delocalized plasmons in metallic nanovoids. *Phys. Rev. B* **74**, 245415 (2006).
45. Viguerie, L., Walter, P., Laval, E., Mottin, B. & Sole, V. A. Revealing the sfumato technique of Leonardo da Vinci by X-ray fluorescence spectroscopy. *Angew. Chem. Int. Ed.* **49**, 6125–6128 (2010).
46. Kudyshev, Z. A., Kildishev, A. V., Shalaev, V. M. & Boltasseva, A. Machine-learning-assisted metasurface design for high-efficiency thermal emitter optimization. *Appl. Phys. Rev.* **7**, 021407 (2020).
47. Ma, W. et al. Deep learning for the design of photonic structures. *Nat. Photon.* **15**, 77–90 (2021).
48. Wiecha, P. R., Lecestre, A., Mallet, N. & Larrieu, G. Pushing the limits of optical information storage using deep learning. *Nat. Nanotechnol.* **14**, 237–244 (2019).
49. Dong, Z. et al. Schrödinger's red pixel by quasi-bound-states-in-the-continuum. *Sci. Adv.* **8**, eabm4512 (2022).

Methods

Optical characterization

The colours of the metasurface were characterized by using a bright field reflection microscope set-up (Zeiss Axio Observer) illuminated by a white light source. A chromatic CCD camera (Zeiss AxioCam MRc5) was used to photograph the colour images. The reflectance spectra are measured using an ultraviolet–infrared–near infrared microspectrophotometers (CRAIC PV20/30).

Fabrication of metasurface

First, a silicon wafer was ultrasonically cleaned successively using acetone, chloroform, ethyl alcohol and deionized water. The wafer was then boiled in a H_2SO_4·H_2O_2 (3:1) solution for 60 min and cleaned in deionized water, alcohol and acetone in sequence. Then the AR-3170 positive photoresist (PR) was spin coated onto the silicon substrate at a speed of 4,000 r.p.m. and baked for 10 min at 100 °C. The thickness of the PR was about 120 nm as measured by a surface profiler. The PR was patterned by electron beam lithography. After exposure, the periodically patterned PR can be obtained after development in an AR 300–35 solution. Then reactive-ion etching was used to transfer the grating to the silicon substrate with a thickness of 40 nm. Next, the PR on the patterned silicon was removed by acetone and treated with an O_2 plasma. A self-assembled layer of 1H,1H,2H,2H-perfluorooctyltriethoxysilane molecules was subsequently coated on the silicon surface by using a physical vapour deposition method. A layer of silver with a thickness of 1 μm was then deposited on the silicon mould by electron-beam evaporation. Afterwards, the exposed surface of the silver film was glued to a glass slide with an ultraviolet curable epoxy resin adhesive (NOA63), which is then cured ultraviolet light for 15 min. Finally, the patterned silver film together with the glass slide was physically stripped off from the silicon mould due to the weak adhesion between the silver and silicon. As a result, a smooth silver film decorated with a 40-nm-thick nanoaperture array was fabricated.

Data availability

The authors declare that data supporting the findings of this study are available within the article and its Supplementary Information files. All the relevant data are available from the corresponding author upon request.

Acknowledgements

We acknowledge support from the Key Research and Development Program of the Ministry of Science and Technology of China (2017YFA0303700 to Y.L. and T.X.), National Natural Science Foundation of China (62005117 to M.S.), the Natural Science Foundation of Jiangsu Province (BK20220068 to T.X. and BK20212004 to Y.L.) and the Fundamental Research Funds for the Central Universities (to T.X.).

Author contributions

M.S. and T.X. conceived the idea. M.S. performed all the numerical simulations and imaging experiments. L.F. fabricated all the samples. P.H., M.L. and C.H. provided help with the fabrication and experiments. F.Y., Y.L. and T.X. supervised the project. All the authors discussed results and edited the manuscript.

Competing interests

The authors declare no competing interests.

Additional information

Supplementary information The online version contains supplementary material available at https://doi.org/10.1038/s41565-022-01256-4.

Correspondence and requests for materials should be addressed to Yan-qing Lu or Ting Xu.

Peer review information *Nature Nanotechnology* thanks Jay Guo, Joel Yang and the other, anonymous, reviewer(s) for their contribution to the peer review of this work.